



Cite this: DOI: 10.1039/d2sm00725h

## Ion channels in sulfonated copolymer-grafted nanoparticles in ionic liquids†

Ruhao Li, Yuke Han and Pinar Akcora \*

The use of ionic liquids as solvents for polymers or polymer-grafted nanoparticles provides an exciting feature to explore electrolyte–polymer interactions. 1-Hexyl-3-methylimidazolium bis(trifluoromethylsulfonyl)imide (HMIm–TFSI) can have specific interactions with the polymer through ion-dipole forces or hydrogen bonding. In this work, poly(methyl methacrylate)-*b*-poly(styrene sulfonate) (PMMA-*b*-PSS) copolymer-grafted Fe<sub>3</sub>O<sub>4</sub> nanoparticles with different sulfonation levels (~4.9 to 10.9 mol% SS) were synthesized, and their concentration dependent ionic conductivities were reported in acetonitrile and HMIm–TFSI/acetonitrile mixtures. We found that conductivity enhancement with the particle concentration in acetonitrile was due to the aggregation of grafted particles, resulting in sulfonic domain connectivity. The ionic conductivity was found to be related to the effective hopping transfer within ionic channels. On the contrary, the conductivity decreased or remained constant with increasing particle concentration in HMIm–TFSI/acetonitrile. This result was attributed to the ion coupling between ionic liquids and copolymer domains.

Received 1st June 2022,  
Accepted 28th June 2022

DOI: 10.1039/d2sm00725h

[rsc.li/soft-matter-journal](http://rsc.li/soft-matter-journal)

## Introduction

Room temperature ionic liquids (RTILs) have a low melting point, yet maintain extremely low vapor pressure and non-volatility. RTILs have high ion density and conductivity and are used as electrolytes for energy storage devices,<sup>1–3</sup> actuators<sup>4–8</sup> and nanoparticle stabilizers.<sup>9–11</sup> By mixing ILs with non-ionic diblock copolymers, solvation and specific interactions between polymers and ILs can be utilized to enhance the ionic conductivity.<sup>12–14</sup> Furthermore, copolymer morphologies and the ionic mobility of ILs within hydrophilic phases of copolymers have been investigated to understand these hybrid materials.<sup>15,16</sup> Interface and domain orientation were found to influence the ion transport in the imidazolium-based IL incorporated poly(methyl methacrylate) (PMMA)-*b*-polystyrene (PS) diblock copolymer system.<sup>16</sup>

We have studied 1-hexyl-3-methylimidazolium bis(trifluoromethylsulfonyl)imide (HMIm–TFSI) incorporated PMMA-grafted nanoparticles in our previous studies.<sup>12–14,17</sup> Different particle aggregation states were found to influence the dynamics of imidazolium cations,<sup>14</sup> which was measured by quasi-elastic neutron scattering experiments. This was possible as the incoherent scattering signal was coming mostly from the HMIm<sup>+</sup> and the PMMA chains were deuterated and TFSI<sup>–</sup> anions contain no hydrogen. The ion-pair disassociation effect due to ion-dipole interactions between methyl groups of PMMA and TFSI<sup>–</sup> anions

of HMIm–TFSI resulted in increasing the number of free HMIm<sup>+</sup> cations and the ionic conductivity.<sup>13</sup> It was also observed that the long-range unrestricted diffusion of HMIm<sup>+</sup> cations was enhanced in the well-dispersed grafted nanoparticles compared to the neat ILs.<sup>14,18</sup> The preferential interaction between PMMA and TFSI<sup>–</sup> anions also contributed to the solvation of ILs with the addition of solvents. Solvents with high dipole moments such as acetonitrile, acetone and methanol exhibited high ionic conductivity when mixed with ILs. Acetonitrile, with the highest polarity among several solvents tested, showed the highest conductivity when mixed with equal mass of ILs.<sup>17</sup> Thus, the complex solvation induced by ion-dipole interactions between PMMA and ILs influences the overall ion mobility and ionic conductivity of IL/solvent mixtures containing PMMA-grafted nanoparticles.<sup>12,14,17</sup>

In block copolymers of PMMA-*b*-poly(styrene sulfonate) (PSS) mixed with HMIm–TFSI, additional interactions between PSS and HMIm<sup>+</sup> by Coulombic forces co-exist with the solvated IL through interactions between PMMA and TFSI<sup>–</sup>.<sup>14,19</sup> We have found that PMMA-*b*-PSS-grafted nanoparticles with the lower sulfonation amount (0.1 mol% SS) and the longer PMMA chains (398 kDa) exhibited the highest conductivity in acetonitrile and HMIm–TFSI mixtures compared to the particles with the higher sulfonation amount (3 mol%) and the shorter PMMA chains (123 kDa).<sup>13</sup> The high conductivity of the low sulfonated sample was explained by the asymmetric counterion distributions of ILs, where a higher portion of TFSI<sup>–</sup> anions interacted with the longer PMMA chains. The ion–polymer coupling in both copolymer domains facilitates the disassociation of ILs. TOA-protected SS groups and possible coupling of SS groups with

Department of Chemical Engineering and Materials Science, Stevens Institute of Technology, Hoboken, NJ 07030, USA. E-mail: [pakcora@stevens.edu](mailto:pakcora@stevens.edu)

† Electronic supplementary information (ESI) available. See DOI: <https://doi.org/10.1039/d2sm00725h>

**HMIm<sup>+</sup>** cations enhance the solubility of particles in HMIm-TFSI.

In this work, we prepared copolymers with various sulfonate amounts to further understand the solvation and interactions of the HMIm-TFSI with the PMMA-*b*-PSS copolymer. These interactions can result in aggregated strings or networks of strings as the copolymer composition and the particle concentration are varied. Furthermore, the aggregation of ionic clusters can be constrained *via* the disassociation of ILs with the preferential interactions of each counterion with the copolymer domains. Herein, we report the aggregation of copolymer-grafted nanoparticles at a moderately wide range of sulfonation levels (4.86–10.82 mol% SS). The ILs which are associated with the chains differently in various copolymer compositions are examined using impedance spectroscopy, and the measured ionic conductivities are analyzed by the percolation theory. Our results show that the percolation of sulfonated domains in particle-based ion conductors is essential to foster conductivity in particle-based ion conductors.

## Experimental section

### Preparation of particles

Fe<sub>3</sub>O<sub>4</sub> nanoparticles (NPs) were prepared *via* solvothermal reduction of iron(III) acetylacetone [Fe(acac)<sub>3</sub>] with 1,2-tetradecanodiol as the reducing agent.<sup>20</sup> Oleic acid and oleylamine were used as surfactants that cease the growth and ripening of Fe<sub>3</sub>O<sub>4</sub> grains during the reaction and render the product compatibility with benzyl ether. Grafted NPs were drop-cast on Formvar grids for imaging. Fe<sub>3</sub>O<sub>4</sub> NPs of 7 nm in diameter were imaged using a transmission electron microscope (JEOL 2100 Plus S TEM) at 200 kV. Later, oleic acid and oleylamine on NPs were replaced by the chain transfer agent, 4-cyano-4-(phenylcarbonothioylthio)-pentanoic acid (CPDB). The anchoring of CPDB on Fe<sub>3</sub>O<sub>4</sub> NPs is based on the reported procedure,<sup>21</sup> which was slightly modified with reduced CPDB amount and a longer reaction time. Equal volumes of 10 mg mL<sup>-1</sup> Fe<sub>3</sub>O<sub>4</sub>/tetrahydrofuran (THF) and 20 mg mL<sup>-1</sup> CPDB/THF were mixed to react for 72 h by magnetic stirring. Particles were precipitated in cyclohexane and ethyl ether mixture by centrifuging at 4000 rpm for 15 min and redissolved in THF. CPDB anchoring on NPs is confirmed by Fourier transform infrared (FTIR, Bruker Optics Tensor 27) spectroscopy (Fig. S1, ESI<sup>†</sup>). The amount of CPDB is measured using a thermogravimetric analyzer (Q50 TGA, TA Instruments).

### SI-RAFT Polymerization of PMMA-*gr*-Fe<sub>3</sub>O<sub>4</sub>

PMMA chains were grown from CPDB-functionalized NPs by surface-initiated reversible addition-fragmentation chain-transfer (SI-RAFT) polymerization,<sup>22</sup> by which the chain length and graft density can be controlled by monomer, initiator and CTA amounts (Fig. S2, ESI<sup>†</sup>). The grafting of PMMA is confirmed by FTIR (Fig. S3, ESI<sup>†</sup>) and the amount of surface ligands (CPDB and PMMA) and graft density were measured by TGA. Concentrated HCl was added to the PMMA-grafted nanoparticle solution (10 mg mL<sup>-1</sup> in 5 mL THF) to etch the Fe<sub>3</sub>O<sub>4</sub> NPs, and the

mixture solution was sonicated till the solution became clear. Methanol was later added, and the mixture was centrifuged at 6000 rpm for 10 min. The precipitated PMMA chains were dried in vacuum at room temperature to remove methanol, THF, HCl, and water. Finally, the product was redissolved in toluene. The weight-averaged molecular masses of grafted PMMA chains were measured using a gel permeation chromatography-light scattering (GPC/LS) device after etching the particles.

The GPC/LS system in our laboratory is equipped with a VARIAN PL 5.0 μm Mixed-C gel column (7.5 mm ID), a light scattering detector (miniDawn, Wyatt Technology) and a refractive index (RI) detector (Optilab rEX, Wyatt). Averaged molecular masses of synthesized PMMA were measured as 67 kDa (*D*: 1.45) and 122 kDa (*D*: 1.53). Grafting density (GD) was determined through TGA using the following equation:

$$GD = \frac{m_{\text{polymer}}}{m_{\text{NP}}} \frac{N_A \rho R}{3 \bar{M}_w} \quad (1)$$

*m*<sub>polymer</sub> and *m*<sub>NP</sub> are the mass of grafted chains and particle cores, respectively. *N*<sub>A</sub> is the Avogadro constant; *ρ* is the particle density; *R* is the radius of iron oxide nanoparticles; and *ℳ*<sub>w</sub> is the weight-averaged molecular weight of grafted chains.

### Preparation of trioctylammonium *p*-styrenesulfonate (SS-TOA)

Trioctylammonium (TOA) capping was necessary to produce the hydrophobic SS-TOA monomer. TOA capped *p*-styrenesulfonate (SS-TOA) was prepared following the published procedure.<sup>23,24</sup> TOA protection solubilized the copolymer-grafted particles in toluene.

### Synthesis of PMMA-*b*-PSSTOA-grafted nanoparticles

SS monomer was sequentially added to the living PMMA chains (Fig. 1). The CTA, initiator, and monomer amounts used to synthesize the sulfonated copolymer particles are given in Table S2 (ESI<sup>†</sup>).

Hydrodynamic sizes of grafted particles before and after sulfonation were measured in dynamic light scattering (DLS, Zetasizer NanoS, Malvern). PSS amounts were determined by the end-group analysis using <sup>1</sup>H NMR (Varian-400 spectrometer). The chemical shift was recorded in the unit of parts per million (ppm) and was calibrated by CDCl<sub>3</sub> at 7.26 ppm.

### Electrochemical impedance spectroscopy (EIS)

The SP-300 electrochemical impedance spectrometer, Bio-Logic Science Instruments, was used for EIS measurements. The samples were tested in a home-made liquid cell with stainless steel electrodes. The Nyquist plots, frequency-dependent conductivity and ionic conductivity were acquired by AC with 10 mV amplitude at the 7 MHz–1 Hz frequency range. The Nyquist plot was fitted by an equivalent circuit (EC) with the ZView software. The frequency dependence of bulk conductivity is plotted in Fig. S4 (ESI<sup>†</sup>). Ionic conductivities (σ') were obtained from the high-frequency plateau, where ionic mobility dominates the impedance spectra.<sup>25</sup> The bulk conductivity

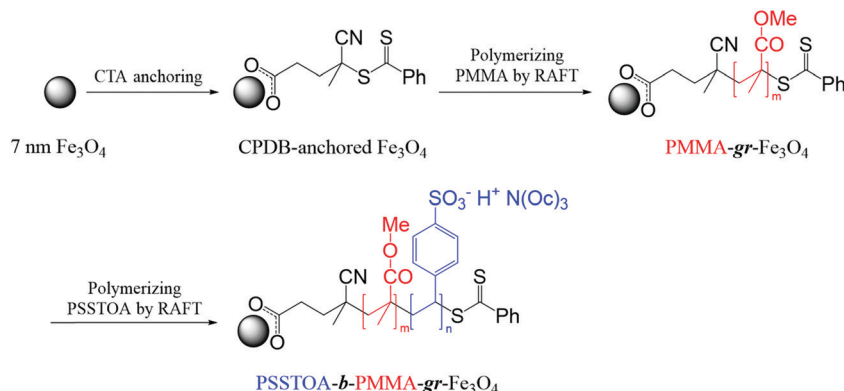


Fig. 1 Synthesis of PSSTOA-*b*-PMMA-grafted  $\text{Fe}_3\text{O}_4$  nanoparticles by RAFT polymerization.

$\sigma'(\omega)$  was calculated as per the following eqn (2).<sup>12</sup>

$$\sigma'(\omega) = \frac{Z'}{k[(Z')^2 + (Z'')^2]} \quad (2)$$

where  $\omega$  is the angular frequency,  $Z'$  and  $Z''$  are the real and imaginary parts of impedance, respectively,  $k$  is the cell constant which was determined using a 0.01 M KCl standard solution (Ricca Chemical, 1412  $\mu\text{S cm}^{-1}$  at 25 °C).

## Results and discussion

We have synthesized PMMA-grafted chains of 67 kDa (in Samples 1–3) and used them to polymerize PSS chains at varying lengths and at sulfonation levels between 6.05 and 10.82 mol% SS, and we prepared another grafted Sample 4 with 122 kDa PMMA chains at 4.86 mol% SS (Fig. 2).

The stoichiometric percentage of SS was calculated by

$$[\text{SS}]\% = \frac{n_{\text{SS}}}{n_{\text{MMA}} + n_{\text{SS}}} \times 100\% \quad (3)$$

where  $n_{\text{SS}}$  and  $n_{\text{MMA}}$  are the molar amounts of SS and MMA monomers in the copolymer chain, respectively.

The sample characteristics of  $\bar{M}_w$  and  $\overline{DP}_w$ , PMMA/ $\overline{DP}_w$ , PSSTOA ( $m/n$ ) are given in Table 1. The molar ratio of blocks ( $m/n$ ) varies between 8.3 and 19.7. Samples 1–3 are at lower graft density (GD: 0.15 chains  $\text{nm}^{-2}$ ), and Sample 4 has GD: 0.69 chains  $\text{nm}^{-2}$ . The GD values are much larger than the  $1/R_g^2$  of 67 kDa and 122 kDa PMMA chains, indicating the high graft density of chains around particles.

$^1\text{H}$  NMR is used to calculate the sulfonation level of copolymers after etching the NPs (Fig. 2c). Peaks at 7.2 ppm and 3.6 ppm are originated from the aromatic *ortho*-hydrogen on the PSSTOA block and methyl hydrogen on the PMMA block,

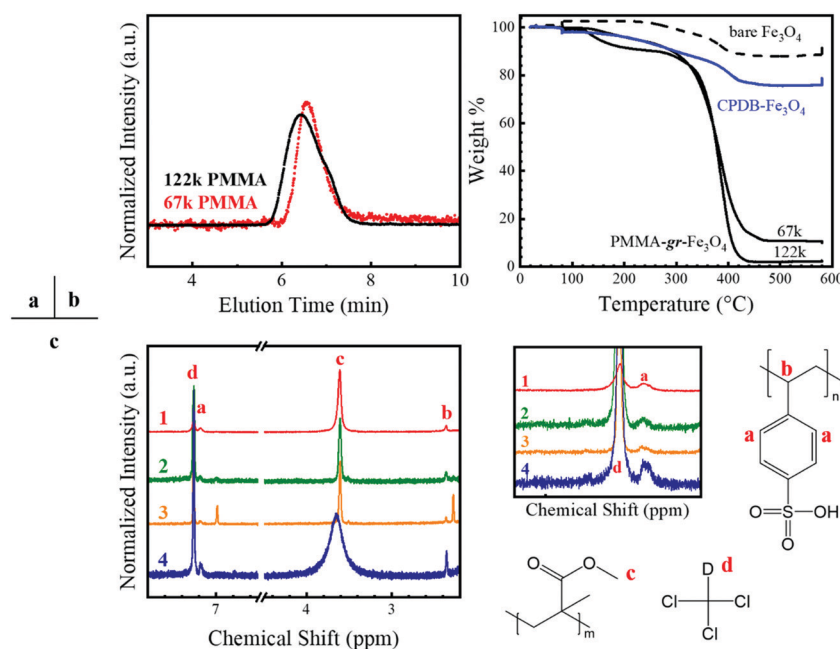


Fig. 2 (a) GPC-LS traces of 67 kDa and 122 kDa PMMA. (b) TGA data of the PMMA-grafted, the bare and CPDB-anchored  $\text{Fe}_3\text{O}_4$  NPs. (c)  $^1\text{H}$  NMR spectra of PMMA-*b*-PSSTOA copolymers (Samples 1–4).

**Table 1** Characteristics of  $\text{PMMA}_m-b\text{-PSSTOA}_n$  grafted  $\text{Fe}_3\text{O}_4$  nanoparticles

Sample	$\bar{M}_{w,\text{PMMA}}$ (kDa)	$\overline{DP}_{w,\text{PMMA}}(m)$	$D$	GD (chains $\text{nm}^{-2}$ )	SS% (mol%)	$\overline{DP}_{w,\text{PSSTOA}}(n)$	$m/n$
1	67.0	669	1.45	0.15	6.05	43	15.6
2	67.0	669	1.45	0.15	9.42	70	9.6
3	67.0	669	1.45	0.15	10.82	81	8.3
4	122	1219	1.53	0.69	4.86	62	19.7

respectively. The ratio of integrated areas ( $A_{\text{PSSTOA}}/A_{\text{PMMA}}$ ) for the PSSTOA and PMMA is directly proportional to the number of hydrogens ( $N_{\text{H,PSSTOA}}, N_{\text{H,PMMA}}$ ) per monomer, as shown in the following equation:

$$\frac{A_{\text{PSSTOA}}}{A_{\text{PMMA}}} = \frac{n_{\text{SS}} N_{\text{H,PSSTOA}}}{n_{\text{MMA}} N_{\text{H,PMMA}}} \quad (4)$$

The integrated areas of all samples calculated prior to the intensity normalization are listed in Table S1 (ESI†).

All sulfonated samples have larger hydrodynamic sizes than their homopolymer precursors as shown in Fig. 3a. Within Samples 1–3, the hydrodynamic size increased from 100 nm to 225 nm as SS% is changed from 6.05 to 10.82 (Fig. 3b). In Sample 4, the high GD provides a stronger steric repulsion and particles have lower hydrodynamic sizes than Samples 1–3. TEM data show aggregated structures at all sulfonation levels. Samples were solution cast from toluene on grids. Sample 3 with the highest sulfonation amount showed the highly aggregated structures (Fig. 3c). Good dispersion in Sample 4 is not surprising due to its strong steric repulsion of high GD chains.

The distribution of  $\text{TFSI}^-$  anions around grafted particle aggregates is visualized by scanning electron microscopy (SEM)

and energy dispersive X-ray spectroscopy (EDS) (Fig. 4). The Fe mapping easily locates the  $\text{Fe}_3\text{O}_4$  NP cores. The dense fluoride (F) signal on the  $\text{Fe}_3\text{O}_4$  shows the  $\text{TFSI}^-$  anion distribution because  $\text{TFSI}^-$  is the only molecule containing F. The S signals on the other hand are denser in the outer regions of  $\text{Fe}_3\text{O}_4$ , and they are attributed to PSS. The N signal matches the S mapping, revealing that it is from the  $\text{HMIm}^+$ . This matching between N and S signifies the affinity between  $\text{HMIm}^+$  cations and the PSS block. While these results are qualitative, they help us to demonstrate the preferential interactions between cations and PSS as well as between anions and PMMA.

Copolymer samples 1–4 in acetonitrile at different concentrations were tested by EIS for conductive properties. The Nyquist plot shows the impedance in a complex plane. The shape of a typical Nyquist plot of an electrolyte solution contains Warburg impedance at lower frequency regions and single or multiple arcs at higher frequencies. The Warburg impedance is originated from the diffusion of ions and appears linear.<sup>26</sup> The arcs are attributed to both resistive and capacitive behaviors, which can be further explained by ion transfer, dielectric constant at the electrode–electrolyte interface.<sup>27</sup> Ionic conductivity ( $\sigma'$ ) is averaged from the AC frequency-dependent bulk conductivity in the plateau region, and the latter is

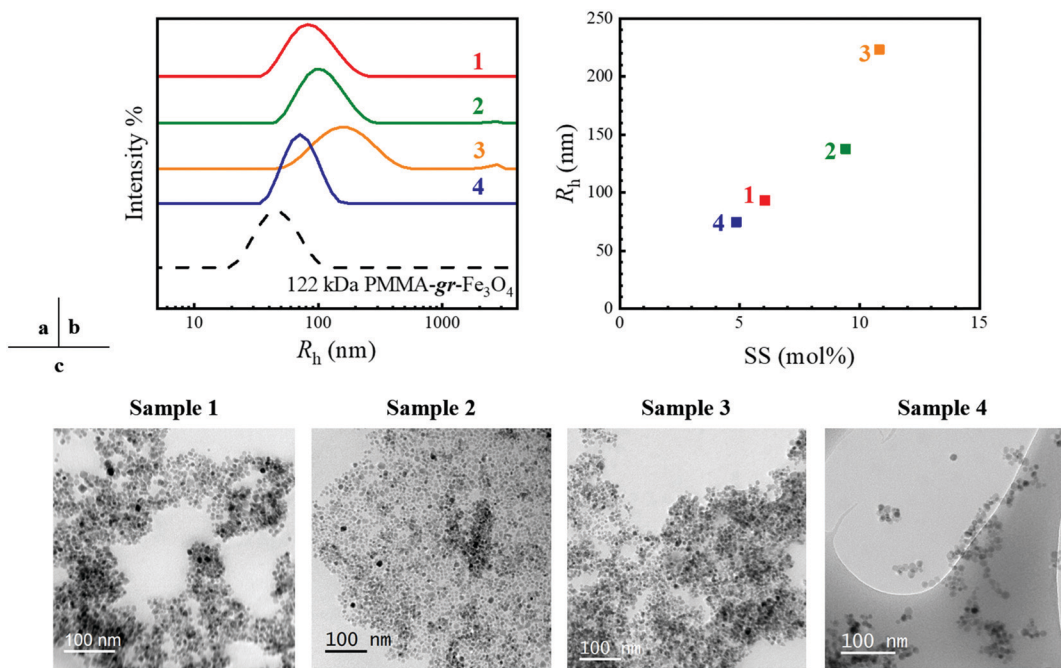


**Fig. 3** (a) Z-averaged hydrodynamic size  $R_h$  distributions of all samples in toluene. (b)  $R_h$  of samples with varying SS mol% in toluene. (c) TEM data of  $\text{PMMA}_m-b\text{-PSSTOA}_n$  grafted NPs.

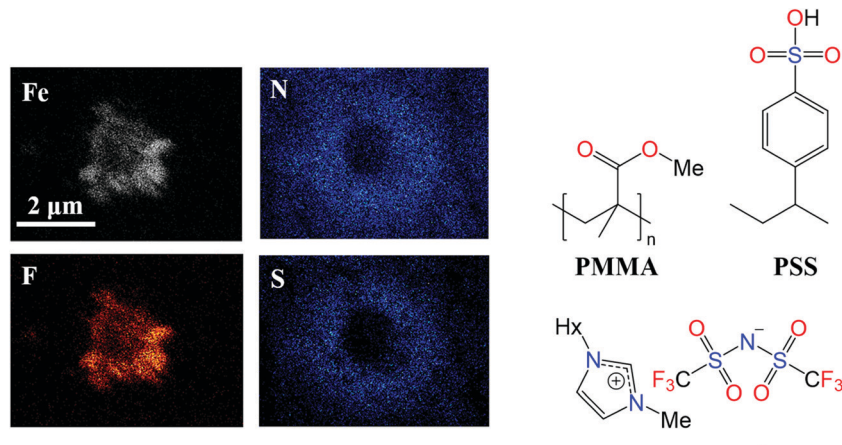


Fig. 4 SEM-EDS data of PMMA-*b*-PSS copolymer-grafted  $\text{Fe}_3\text{O}_4$  NPs for Fe, F, N and S element mappings, and the chemical structures of species.

calculated from the Nyquist plot *via* eqn (2). Fig. 5 shows the ionic conductivity dependence on the volume fraction of PSS. Sample 4 with high GD (0.69 chains  $\text{nm}^{-2}$ ) has lower conductivity than the other samples in acetonitrile. The conductivity increased sharply at low concentrations and then reached to more-like plateau values. We thus estimated the percolation threshold ( $\Phi_c$ ) to be 0.001%, suggesting the percolating structure occurs at a slightly lower concentration than our experiment range. The apparent enhancement in conductivity values with the increasing sulfonation amount was seen at high concentrations. Polymer ( $f_{\text{polymer}}$ ) and PSSTOA ( $f_{\text{SSTOA}}$ ) volume fractions are calculated using the equations:

$$f_{\text{polymer}} = \frac{Cw}{\rho_{\text{PMMA}}}, \quad f_{\text{NP}} = \frac{C(1-w)}{\rho_{\text{NP}}} \quad (5)$$

$$f_{\text{SSTOA}} = f_{\text{NP}}x \quad (6)$$

$C$  is the mass concentration of polymer-grafted nanoparticles and  $w$  is the weight loss fraction of polymer-grafted NPs;  $\rho_{\text{PMMA}}$

and  $\rho_{\text{NP}}$  are densities of PMMA and  $\text{Fe}_3\text{O}_4$ , respectively; and  $x$  is the sulfonation molar fraction.  $\Phi_{\text{SSTOA}}$ ,  $\Phi_{\text{PGNP}}$ ,  $\Phi_{\text{polymer}}$  are volume percentages of PSSTOA, PMMA-*b*-PSSTOA-grafted NPs and PMMA-*b*-PSSTOA, respectively.

We plotted the conductivity *versus*  $\Phi_{\text{PGNP}} - \Phi_c$  and fitted to a  $\sigma' = \sigma_0 (\Phi_{\text{PGNP}} - \Phi_c)^t$  equation that describes the percolation model of the infinite-size network connectivity.<sup>28</sup> The linear fittings of the conductivity are ascribed to particle connectivity (Fig. 6a).  $\Phi_c$  is the percolation threshold, and  $t$  is the critical exponent that depends on the connectivity of nanoparticles and it is the slope of the linear fitting line. The geometric percolation threshold of hard spheres is reported to be 0.297.<sup>21</sup> The threshold  $\Phi_c$  depends on aspect ratio and can be low (0.001 vol%) for anisotropic nanofillers such as carbon nanotubes and carbon black.<sup>29-31</sup> The percolation threshold of our grafted particles is much lower than that of hard spheres as grafted particles have large hydrodynamic sizes (Fig. 3). The interfacial stretching in PMMA-*b*-PSS<sup>32</sup> and the anisotropic self-assembly of particles<sup>33,34</sup> are other ruling phenomena that govern the aggregation of grafted particles. Another important factor is the electric percolation threshold occurring at a lower concentration than the mechanical percolation threshold as the ions hop between localized particle aggregates.<sup>30</sup> The exponent  $t$  is found to be around 0.6 in Samples 1–3 indicating a similarity to their network topologies (Table S3, ESI†).

It is important to note that the sharp increase of ionic conductivity was not seen for bare NPs and PMMA-grafted NPs (Fig. S5, ESI†). We compared the particle-grafted samples with the SSTOA monomer (Fig. 5, purple open dots). In SSTOA, ions freely diffuse as there is no structure effect or ion coupling to the polymer. The ionic conductivity of SSTOA is expected to be higher than that of polymer-grafted NPs, but was measured to be lower than all the 3 samples. Thus, the high conductivity in Samples 1–3 with low GD was attributed to the percolating structures as illustrated in Fig. 6b. The steric repulsion of Sample 4 with high GD hinders entanglements between ionic groups of PSS. The relatively lower value of  $t$  (0.542) signifies the lowest connectivity, and the lowest value of  $R^2$  represents a low explanatory power of percolation theory for this

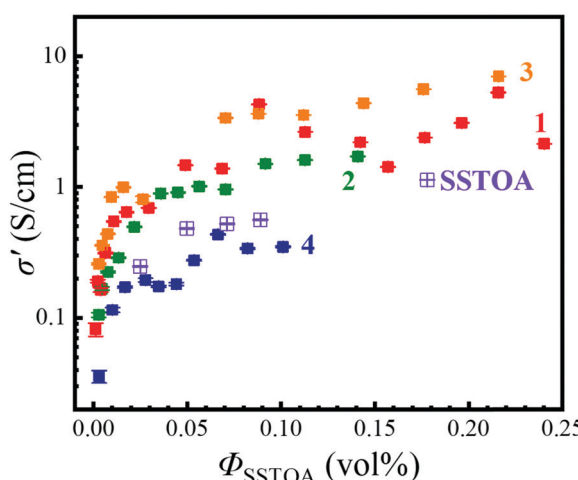


Fig. 5 Ionic conductivities ( $\sigma'$ ) of PMMA-*b*-PSS-grafted  $\text{Fe}_3\text{O}_4$  NPs (Samples 1–4) and SSTOA monomer in acetonitrile with varying PSS volume percentages ( $\Phi_{\text{SSTOA}}$ ).

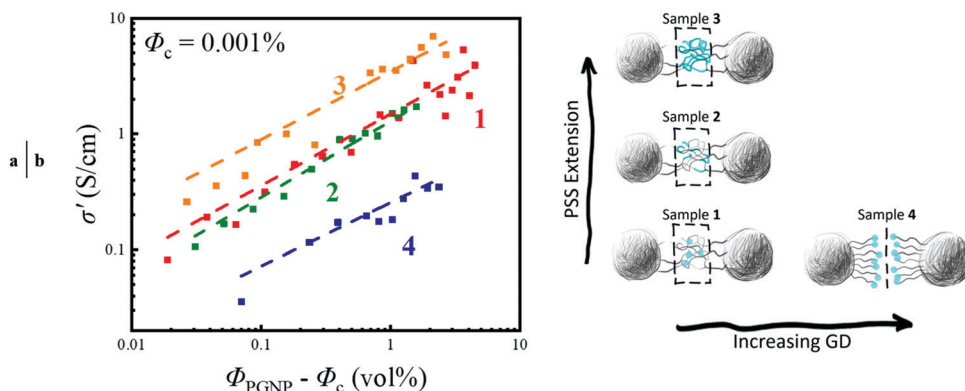


Fig. 6 (a) Ionic conductivity ( $\sigma'$ ) of PMMA-*b*-PSS copolymer-grafted NPs in acetonitrile as a function of the volume percentage,  $\Phi_{\text{PGNP}} - \Phi_c$ . (b) Schematic illustration of ionic connectivity between PMMA-*b*-PSS-grafted NPs for varying sulfonation amount in SS% (Samples 1–3) and graft density (Samples 1 and 4). The cyan parts refer to PSS blocks.

sample (Table S3, ESI†). Interestingly, Sample 4 has lower ionic conductivity than the SSTOA monomer.

Furthermore, we used equivalent circuit (EC) models to analyze the impedance data of copolymer-grafted NPs in acetonitrile. Two EC models (Fig. S6, ESI†) numerically reproduce the Nyquist plots for the low and high conductivity ranges (Fig. S7, ESI†). The values of circuit elements ( $R_1$ ,  $C_1$  and CPE<sub>1</sub>) are related to the polymer-grafted nanoparticle concentration. The  $R_1$  element refers to the resistance of ions moving through the bulk electrolyte<sup>35</sup> and decreases with the particle concentration (Fig. S8a, ESI†). Sample 3 has the strongest concentration dependence of  $R_1$  value, and Sample 4 has the weakest. The other elements ( $C_1$  and CPE<sub>1</sub>) refer to the capacitance and increase with concentration in Samples 1–3 unlike Sample 4 (Fig. S8b and c, ESI†). The ion transport in Samples 1–3 enhances by the percolated sulfonated domains within the aggregated particles. Sample 4 does not exhibit this behavior because it does not form such effective networks. We note that the vehicular diffusion of free TOA<sup>+</sup> ions in acetonitrile has a minor effect on the conductivity.

On the contrary, we observed that the conductivity of particles dispersed in HMIm-TFSI/acetonitrile decreased with concentration (Fig. 7a). The coupling of PMMA with TFSI<sup>–</sup> and PSS with HMIm<sup>+</sup> reduces the free ion concentration, hence diffusion. Such interactions solvate the IL and aid in better dispersion in HMIm-TFSI (Fig. S9, ESI†) compared to that in acetonitrile as shown in Fig. 3. Since both blocks of copolymer impair ion motion, increasing the polymer concentration ( $\Phi_{\text{polymer}}$ ) lowers the free ion conductivity in Samples 1 and 4. In Samples 2 and 3 that can form a network by their longer chain and lower graft density, ionic conductivities decrease only slightly. At very low concentrations, Samples 1 and 3 have higher conductivity than the neat IL/acetonitrile. The decline of conductivity with particle concentration increase suggests that ion coupling of polymers becomes effective in Samples 1 and 3. The conductivity of ions that are coupled with PMMA and PSS balances out the high conductivity that is for the low particle concentration. Percolation is stronger in Sample 1 compared to Sample 4 and the large decrease in conductivity of Sample 4 is attributed to the weaker connectivity of PSS domains.

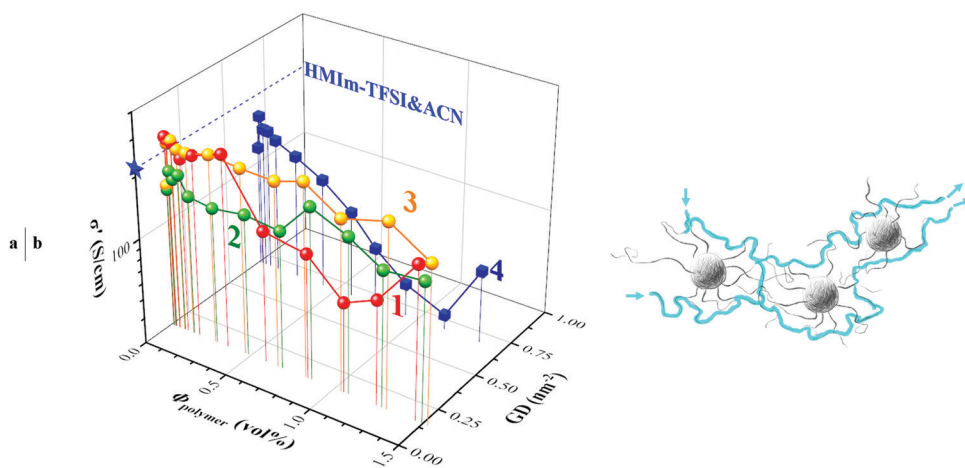


Fig. 7 (a) Ion conductivities of copolymer-grafted NPs in HMIm-TFSI/acetonitrile (ACN) for varying polymer concentration,  $\Phi_{\text{polymer}}$ . The data point shown with a star is for the neat HMIm-TFSI/ACN. (b) Sulfonated chain percolation is represented with an illustrative work of aggregated grafted nanoparticles.

## Conclusions

A series of PMMA-*b*-PSS copolymer-grafted  $\text{Fe}_3\text{O}_4$  nanoparticles at varying sulfonation levels were prepared to study the macroscopic ionic conductivities of particles solvated in HMIm-TFSI. It is known that pure HMIm-TFSI conducts ions in a vehicular mode. This work aims to understand how copolymer grafted NPs interfere with the conductivity of HMIm-TFSI. SEM-EDS elemental mapping demonstrates the PMMA-TFSI<sup>-</sup> and PSS-HMIm<sup>+</sup> affinities. Herein, we show that the network of polymer-grafted particles establishes *ion channels* where ions hop through the percolating sulfonated polymer in acetonitrile, which significantly enhances the ionic conductivity with concentration. The equivalent circuit analysis of EIS data also supports that the percolating structures guide ion transport *via* hopping rather than free diffusion. Particles in HMIM-TFSI exhibited an opposite trend where conductivity decreased with grafted polymer concentration. The coupling of each polymer domain with the IL counterparts through ion-dipole interactions led to lower conductivity than that of neat ILs. The low graft density and polymer interactions with ILs can enhance the dispersion state of polymer-grafted nanoparticles, but lower the transport of IL species. In conclusion, polymer-ion coupling and organization of sulfonated domains (in an IL or a solvent) both contribute to the ion transport in grafted-particle based electrolytes.

## Conflicts of interest

There are no conflicts to declare.

## Acknowledgements

This work was supported by the National Science Foundation DMR Polymers program under awards #1807802 and 2104924. We thank Dr. Tsengming Chou for his help with SEM-EDS experiments.

## References

- 1 T. Chen, W. Kong, Z. Zhang, L. Wang, Y. Hu, G. Zhu, R. Chen, L. Ma, W. Yan, Y. Wang, J. Liu and Z. Jin, Ionic liquid-immobilized polymer gel electrolyte with self-healing capability, high ionic conductivity and heat resistance for dendrite-free lithium metal batteries, *Nano Energy*, 2018, **54**, 17–25.
- 2 R. Koyilapu, S. Singha, S. N. R. Kutcherlapati and T. Jana, Grafting of vinylimidazolium-type poly(ionic liquid) on silica nanoparticle through RAFT polymerization for constructing nanocomposite based PEM, *Polymer*, 2020, **195**, 122458.
- 3 K. M. Beers and N. P. Balsara, Design of Cluster-free Polymer Electrolyte Membranes and Implications on Proton Conductivity, *ACS Macro Lett.*, 2012, **1**(10), 1155–1160.
- 4 O. Kim, T. J. Shin and M. J. Park, Fast low-voltage electroactive actuators using nanostructured polymer electrolytes, *Nat. Commun.*, 2013, **4**(1), 2208.
- 5 K. Kruusamäe, A. Punning, A. Aabloo and K. Asaka, Self-Sensing Ionic Polymer Actuators: A Review, *Actuators*, 2015, **4**(1), 17–38.
- 6 O. Kim, H. Kim, U. H. Choi and M. J. Park, One-volt-driven superfast polymer actuators based on single-ion conductors, *Nat. Commun.*, 2016, **7**(1), 13576.
- 7 Q. He, D. Vokoun, T. Stalbaum, K. J. Kim, A. I. Fedorchenko, X. Zhou, M. Yu and Z. Dai, Mechanolectric transduction of ionic polymer-graphene composite sensor with ionic liquid as electrolyte, *Sens. Actuators, A*, 2019, **286**, 68–77.
- 8 V. Palmre, E. Lust, A. Jänes, M. Koel, A.-L. Peikolainen, J. Torop, U. Johanson and A. Aabloo, Electroactive polymer actuators with carbon aerogel electrodes, *J. Mater. Chem.*, 2011, **21**(8), 2577–2583.
- 9 Y. Men, M. Drechsler and J. Yuan, Double-Stimuli-Responsive Spherical Polymer Brushes with a Poly(ionic liquid) Core and a Thermoresponsive Shell, *Macromol. Rapid Commun.*, 2013, **34**(21), 1721–1727.
- 10 B. Kerscher, A.-K. Appel, R. Thomann and R. Mülhaupt, Treelike Polymeric Ionic Liquids Grafted onto Graphene Nanosheets, *Macromolecules*, 2013, **46**(11), 4395–4402.
- 11 K. T. Prabhu Charan, N. Pothanagandhi, K. Vijayakrishna, A. Sivaramakrishna, D. Mecerreyes and B. Sreedhar, Poly(ionic liquids) as “smart” stabilizers for metal nanoparticles, *Eur. Polym. J.*, 2014, **60**, 114–122.
- 12 S. Liu, M. Tyagi and P. Akcora, Polymer-Coupled Local Dynamics Enhances Conductivity of Ionic Liquids, *Macromolecules*, 2020, **53**(15), 6538–6546.
- 13 S. Liu, D. Wu and P. Akcora, Ion-Containing Polymer-Grafted Nanoparticles in Ionic Liquids: Implications for Polymer Electrolyte Membranes, *ACS Appl. Nano Mater.*, 2021, **4**(8), 8108–8115.
- 14 S. Liu, C. Liedel, N. V. Tarakina, N. C. Osti and P. Akcora, Dynamics of ionic liquids in the presence of polymer-grafted nanoparticles, *Nanoscale*, 2019, **11**(42), 19832–19841.
- 15 M. L. Hoarfrost, M. S. Tyagi, R. A. Segalman and J. A. Reimer, Effect of confinement on proton transport mechanisms in block copolymer/ionic liquid membranes, *Macromolecules*, 2012, **45**(7), 3112–3120.
- 16 S. Sharick, J. Koski, R. A. Riggelman and K. I. Winey, Isolating the Effect of Molecular Weight on Ion Transport of Non-Ionic Diblock Copolymer/Ionic Liquid Mixtures, *Macromolecules*, 2016, **49**(6), 2245–2256.
- 17 S. Liu, M. Walton, N. V. Tarakina and P. Akcora, Solvation in Ionic Liquids with Polymer-Grafted Nanoparticles, *J. Phys. Chem. B*, 2020, **124**(23), 4843–4850.
- 18 M. Cai, Q. Yu, W. Liu and F. Zhou, Ionic liquid lubricants: when chemistry meets tribology, *Chem. Soc. Rev.*, 2020, **49**(21), 7753–7818.
- 19 L. Yan, L. Hoang and K. I. Winey, Ionomers from Step-Growth Polymerization: Highly Ordered Ionic Aggregates and Ion Conduction, *Macromolecules*, 2020, **53**(5), 1777–1784.
- 20 S. Sun, H. Zeng, D. B. Robinson, S. Raoux, P. M. Rice, S. X. Wang and G. Li, Monodisperse  $\text{MFe}_2\text{O}_4$  ( $\text{M} = \text{Fe, Co, Mn}$ ) Nanoparticles, *J. Am. Chem. Soc.*, 2004, **126**(1), 273–279.

21 R. Inouibli, S. Dagréou, A. Lapp, L. Billon and J. Peyrelasse, Nanostructure and Mechanical Properties of Polybutylacrylate Filled with Grafted Silica Particles, *Langmuir*, 2006, 22(15), 6683–6689.

22 Y. Jiao and P. Akcora, Accelerated brush growth on nanoparticle surfaces by reversible addition-fragmentation chain transfer polymerization, *J. Polym. Sci., Part A: Polym. Chem.*, 2014, 52(12), 1700–1705.

23 Y. Liu, K. L. Pollock and K. A. Caviechi, Synthesis of poly(triethylammonium p-styrenesulfonate) homopolymers and block copolymers by RAFT polymerization, *Polymer*, 2009, 50(26), 6212–6217.

24 K. A. Caviechi, Synthesis and polymerization of substituted ammonium sulfonate monomers for advanced materials applications, *ACS Appl. Mater. Interfaces*, 2012, 4(2), 518–526.

25 M. Singh, O. Odusanya, G. M. Wilmes, H. B. Eitouni, E. D. Gomez, A. J. Patel, V. L. Chen, M. J. Park, P. Fragouli, H. Iatrou, N. Hadjichristidis, D. Cookson and N. P. Balsara, Effect of Molecular Weight on the Mechanical and Electrical Properties of Block Copolymer Electrolytes, *Macromolecules*, 2007, 40(13), 4578–4585.

26 B.-A. Mei, O. Munteşari, J. Lau, B. Dunn and L. Pilon, Physical Interpretations of Nyquist Plots for EDLC Electrodes and Devices, *J. Phys. Chem. C*, 2018, 122(1), 194–206.

27 H. Ohno and K. Fujita, Ionic Conductivity. *Electrochemical Aspects of Ionic Liquids*, 2005, pp. 75–81.

28 R. Ramasubramaniam, J. Chen and H. Liu, Homogeneous carbon nanotube/polymer composites for electrical applications, *Appl. Phys. Lett.*, 2003, 83(14), 2928–2930.

29 S.-H. Yao, Z.-M. Dang, M.-J. Jiang, H.-P. Xu and J. Bai, Influence of aspect ratio of carbon nanotube on percolation threshold in ferroelectric polymer nanocomposite, *Appl. Phys. Lett.*, 2007, 91(21), 212901.

30 J. J. Richards, J. B. Hipp, J. K. Riley, N. J. Wagner and P. D. Butler, Clustering and Percolation in Suspensions of Carbon Black, *Langmuir*, 2017, 33(43), 12260–12266.

31 J. Li, P. C. Ma, W. S. Chow, C. K. To, B. Z. Tang and J. K. Kim, Correlations between Percolation Threshold, Dispersion State, and Aspect Ratio of Carbon Nanotubes, *Adv. Funct. Mater.*, 2007, 17(16), 3207–3215.

32 H. He, M. Zhong, B. Adzima, D. Luebke, H. Nulwala and K. Matyjaszewski, A Simple and Universal Gel Permeation Chromatography Technique for Precise Molecular Weight Characterization of Well-Defined Poly(ionic liquid)s, *J. Am. Chem. Soc.*, 2013, 135(11), 4227–4230.

33 Q.-H. Wei, M. Han, C.-H. Zhou and N.-B. Ming, Percolation of two-dimensional attractive coagulated particles, *Phys. Rev. E: Stat., Nonlinear, Soft Matter Phys.*, 1994, 49(5), 4167–4171.

34 Y. Jiao and P. Akcora, Assembly of Polymer-Grafted Magnetic Nanoparticles in Polymer Melts, *Macromolecules*, 2012, 45(8), 3463–3470.

35 J. T. S. Irvine, D. C. Sinclair and A. R. West, Electroceramics: Characterization by Impedance Spectroscopy, *Adv. Mater.*, 1990, 2(3), 132–138.